

Accepted Manuscript

The relationship between molecular structure and electronic properties in dicyanovinyl substituted acceptor-donor-acceptor chromophores

Simge Tarkuç, Rienk Eelkema, Ferdinand C. Grozema



PII: S0040-4020(17)30420-9

DOI: [10.1016/j.tet.2017.04.037](https://doi.org/10.1016/j.tet.2017.04.037)

Reference: TET 28638

To appear in: *Tetrahedron*

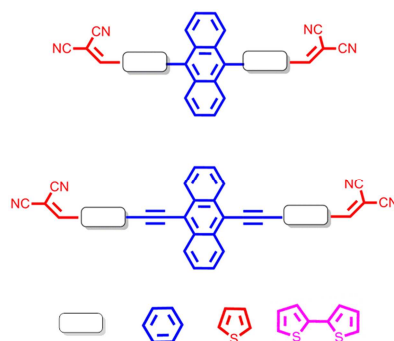
Received Date: 2 March 2017

Revised Date: 14 April 2017

Accepted Date: 15 April 2017

Please cite this article as: Tarkuç S, Eelkema R, Grozema FC, The relationship between molecular structure and electronic properties in dicyanovinyl substituted acceptor-donor-acceptor chromophores, *Tetrahedron* (2017), doi: 10.1016/j.tet.2017.04.037.

This is a PDF file of an unedited manuscript that has been accepted for publication. As a service to our customers we are providing this early version of the manuscript. The manuscript will undergo copyediting, typesetting, and review of the resulting proof before it is published in its final form. Please note that during the production process errors may be discovered which could affect the content, and all legal disclaimers that apply to the journal pertain.



A systematic study of the relation between the molecular structure and the electronic properties of new dicyanovinyl (DCV) substituted acceptor-donor-acceptor chromophores is described. A combination of theoretical and experimental methods shows a subtle relation between the charge transfer character and the geometry of the molecules.

The relationship between molecular structure and electronic properties in dicyanovinyl substituted acceptor-donor-acceptor chromophores

Simge Tarkuç^{a,b,*}, Rienk Eelkema^{b,*} and Ferdinand C. Grozema^{b,*}

^aArçelik A.Ş R&D Center, Material Technologies, Tuzla/Istanbul 34950 Turkey

^bDepartment of Chemical Engineering, Delft University of Technology, Van der Maasweg 9, 2629 HZ Delft, The Netherlands

e-mail: starkuc09@gmail.com, r.eelkema@tudelft.nl, f.c.grozema@tudelft.nl

*Corresponding author

Abstract

In this contribution we describe a combined experimental and theoretical study of the relation between the molecular structure and the electronic properties of conjugated donor-acceptor type chromophores for light-harvesting applications. A series of model systems was synthesized where a central anthracene (electron donor) is connected to dicyanovinyl units (electron acceptor) through a π -conjugated spacer. The study of the redox and optical properties of these chromophores and of reference compounds without dicyanovinyl units allows us correlate the electronic properties to the presence of the electron withdrawing groups and the molecular conformation. Comparison with calculated electronic structure shows that the construction of chromophores that consist of electron donating and accepting units does not always follow the simple rules that are generally used in the design of such molecules. The results show a subtle relation between the charge transfer character and the geometry of the molecules. In some cases this leads to significant contribution of charge transfer excitation to the absorption spectra of some chromophores while such contributions are completely absent in others.

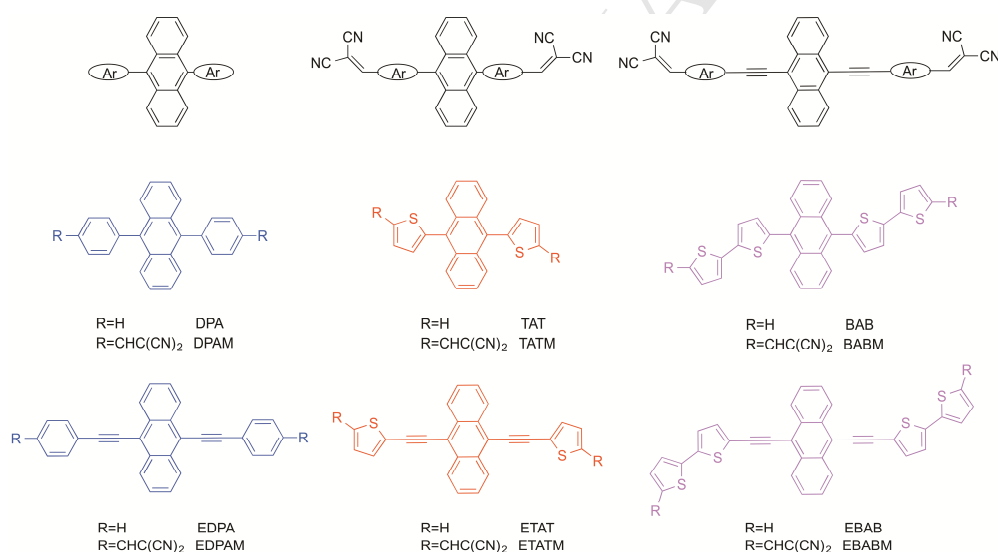
Keywords: small organic dyes, 2,2'-dicyanovinylene, acceptor-donor-acceptor type chromophore, electronic structure, geometry deformation, charge transfer

1. Introduction

Conjugated small molecules and polymers are interesting candidates for application organic opto-electronic devices.¹⁻⁵ One of the attractive points of using such π -conjugated molecules and polymers is that their optical and electronic properties can be optimized for specific applications by using rational design approaches.⁶⁻¹¹ Therefore building a thorough fundamental understanding of the relation between the molecular structure and the electronic properties in such materials is important to provide further guidance for the design of new materials with optimal properties.¹²⁻¹⁴ In this respect, small conjugated model compounds with well-defined geometries prove to be very useful since they allow for a detailed characterization that combines electrochemistry and spectroscopic techniques with high-level theoretical methods. Moreover, small organic molecules are of considerable interest in their own right, for instance for application in photovoltaic devices due to their high absorption coefficient and the possibility to tailor the HOMO-LUMO energy gap.¹⁵⁻²¹ From a synthetic point of view, small organic molecules are attractive since they are monodisperse in nature with well-defined chemical structures and a good batch-to-batch reproducibility. Compared to their polymer counterparts, high-level theoretical studies on small organic molecules can be performed in a relative straightforward manner.

A variety of molecular design approaches have been used to tune the optical properties, charge carrier mobility, HOMO and LUMO energy levels and the structural ordering of small organic molecules in the solid state. One of the most successful approaches to influence the HOMO and LUMO energies involves incorporation of alternating electron-rich (Donor, D) and electron-deficient (acceptor, A) aromatic units into the molecule backbone.²²⁻²⁹ In such combined polymers and oligomers it is assumed that the HOMO of the donor and the LUMO of the acceptor are largely responsible for the location of the frontier orbitals in D-A system.³⁰⁻³¹ The HOMO and LUMO can then be tuned individually, resulting in a straightforward approach to engineer the bandgap of the copolymers/oligomers. While this approach has been predominantly used in polymers, the combination of donors and acceptors in small organic molecules, for instance based on a A- π -D- π -

A configuration, are receiving increasing attention.³²⁻³⁶ This is especially true for the inclusion of dicyanovinyl (DCV) as an electron-withdrawing unit.³⁷⁻³⁹ Recently, a series of oligothiophenes end-capped with such DCV acceptor groups has been developed in the Bäuerle research group.⁴⁰⁻⁴³ It was reported that the introduction of the DCV group leads to a considerably reduced the HOMO-LUMO energy gap and an intense absorption in the visible region due to the strong electron withdrawing nature. The DCV units also contribute to the conjugation of the backbone π -system and can lead to specific intermolecular interactions that change the packing of molecules in the solid state.⁴⁴ In most small organic molecules, acceptor and donor units are linked through a π -spacer to increase the conjugation length. In addition to the length of the π -conjugated spacer, the intrinsic electronic properties of the π -spacer may also affect the spectral response of the molecule.



Scheme 1. Molecular structures of control compounds and DCV-end capped chromophores.

In this contribution, we explore the relation between molecular structure and the electronic properties of small conjugated molecules by considering two series of new model compounds that follow the acceptor-(π -bridge)-donor-(π -bridge)-acceptor architecture (A- π -D- π -A) (Scheme 1). The effects of the acceptor unit on

the optical and electronic properties of the chromophores are investigated and compared to control compounds that lack DCV-units. Within the first series, the aromatic π -spacer is varied from benzene through thiophene to dithiophene, leading to improved optoelectronic properties. In the second series, the changes in the optical and electrochemical behavior originating from the extension of the effective conjugation length by insertion of an ethynyl in the π -bridge are reported. These series of compounds allow us to not only study the effect of combining units with different electronic properties into a single molecule but also to investigate geometrical effects, for instance the planarity of the molecules. The electronic properties have been studied by a combination of experimental methods and electronic structure calculations.

2. Experimental Section

2.1. Material Synthesis.

All starting materials were purchased from Sigma-Aldrich, Acros or Alfa Aesar and used as received without further purification. Analytical thin layer chromatography (TLC) was performed on silica gel 60-F254 (Merck) plates and detected under a UV lamp. Column chromatography was performed on silica gel 60 (Aldrich). 9,10-dibromoanthracene⁴⁵, 5-(5-bromothiophen-2-yl)thiophene-2-carbaldehyde⁴⁶, 9,10-bis((tri-methylsilyl)ethynyl)-anthracene⁴⁷, 9,10-diethynylanthracene (5)⁴⁸, 2-(10-(thiophen-2-yl)anthracen-9-yl)thiophene (TAT)⁴⁹, 2-(thiophen-2-yl)-5-(10-(5-(thiophen-2-yl)thiophen-2-yl)anthracen-9-yl)thiophene(BAB)⁴⁹, 9,10-bis(2-phenylethynyl)anthracene (EBAB)⁵⁰, 2-(2-(10-(2-(thiophen-2-yl)ethynyl)anthracen-9-yl) ethynyl)thiophene (ETAT)⁵¹ were synthesized according to literature procedures.

2.2. Characterization.

¹H NMR and ¹³C NMR spectra were performed in the appropriate deuterated solvents with tetramethylsilane as internal standard on a Bruker Advance spectrometer at 400 MHz (¹H) and 100 MHz (¹³C); chemical shifts (δ) are reported

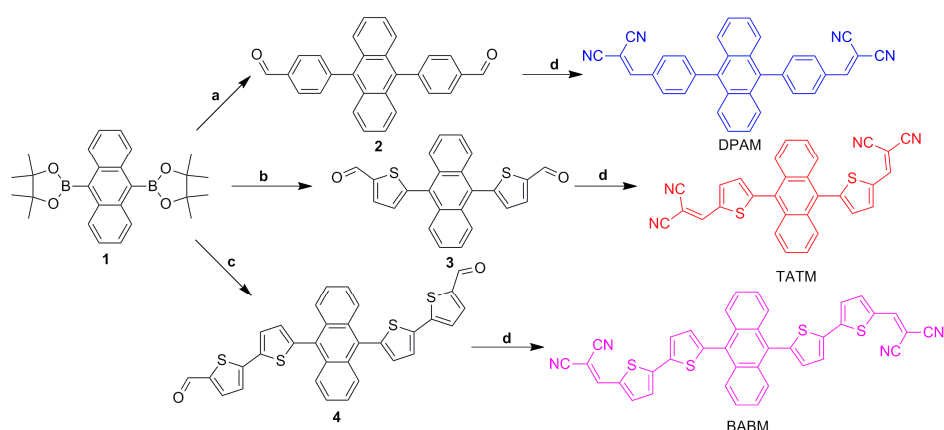
in parts per million. FTIR measurements were carried out on a Perkin Elmer Spectrum One FTIR spectrometer with ATR. EI-MS measurements were performed on a Shimadzu GCMS-QP2010S spectrometer. UV-vis absorption spectra were measured in dichloromethane (CH_2Cl_2) and recorded on a Perkin Elmer Lambda 40 UV-Vis spectrometer. Fluorescence studies were carried out on a QuantaMaster™ 40 UV VIS fluorescence spectrometer.

All electrochemistry experiments were done in a conventional three-electrode cell using a platinum flag working electrode, a platinum wire counter electrode and a silver wire pseudoreference electrode. Cyclic voltammograms were obtained in dry degassed CH_2Cl_2 using 0.1 M tetra-n-butylammonium hexafluorophosphate ($n\text{-Bu}_4\text{NPF}_6$) as the electrolyte, scanning at a rate of 50 mV/s. The electrochemical potential was subsequently calibrated versus the ferrocenium/ferrocene (Fc^+/Fc) using the formal potential of this redox couple as 0.46 V vs SCE in 0.1 M $n\text{-Bu}_4\text{NPF}_6$ in CH_2Cl_2 ⁵²⁻⁴⁸. The corresponding energy levels are reported relative to the vacuum level using the following equations $\text{HOMO} = -(E_{\text{onset,ox vs Fc}^+/\text{Fc}} + 5.1)$ (eV) and $\text{LUMO} = -(E_{\text{onset,red vs Fc}^+/\text{Fc}} + 5.1)$ (eV).

3. Results and Discussion

3.1. Synthesis.

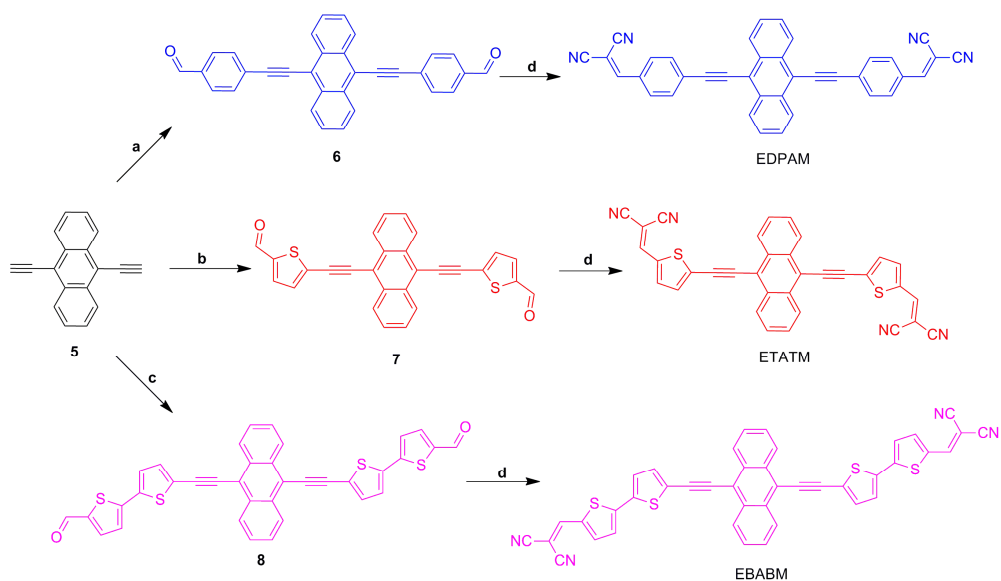
The route to synthesize the acceptor-(π -bridge)-donor-(π -bridge)-acceptor system is depicted in Scheme 2 and 3. Boronic ester **1**, underwent smooth Suzuki cross-coupling with brominated aromatic aldehydes in high conversions under the standard reaction conditions: boronic ester (3 equiv.), sodium hydrogencarbonate (12 equiv.), $\text{Pd}(\text{PPh}_3)_4$ (5 mol %), THF/ H_2O , heating to reflux for 24 h. Subsequent Knoevenagel condensation of the dialdehyde derivatives with malononitrile in the presence of triethylamine resulted in the DCV end-capped target compounds.



Scheme 2. Synthetic routes for directly-linked chromophores (DLCs)^a

^aConditions. (a-c) Pd(PPh₃)₄, THF, K₂CO₃ (aq) (a) 4-bromobenzaldehyde, (b) 5-bromothiophene-2-carbaldehyde, (c) 5-(5-bromothiophen-2-yl)thiophene-2-carbaldehyde, (d) malononitrile, TEA, CHCl₃.

The synthesis of 9,10-bis(ethynylarylaldehyde)anthracene started from anthracene, which was brominated with bromine in acetic acid to give 9,10-dibrominated anthracene. The latter compound was coupled with TMS-acetylene in a Sonogashira coupling reaction to obtain TMS-protected intermediates. The cross-coupling reaction has been performed in TEA with 5 mol % Pd(PPh₃)₂Cl₂ and 10 mol % cuprous iodide at 60 °C for 3 h. The intermediate product was desilylated with 5 equiv. of KOH in a THF/methanol mixture at 25 °C. To obtain the dialdehyde precursors for the DCV-substituted systems, brominated aromatic aldehydes were cross-coupled with deprotected ethynylated intermediates (5) in a Sonogashira reaction with 5 mol % Pd(PPh₃)₂Cl₂ and 10 mol % cuprous iodide at 25 °C for 16 h. In a final step, the dialdehyde derivatives were transformed into the corresponding dicyanovinylene compounds by Knoevenagel condensation with malononitrile in the presence of triethylamine in chloroform. All DCV-substituted systems could be obtained in high purity by flash chromatography on silica gel.



Scheme 3. Synthetic routes for ethynyl-linked chromophores (ELCs)^a

^aConditions. (a-c) Pd(PPh₃)₄, THF, K₂CO₃ (aq) (a) 4-bromobenzaldehyde, (b) 5-bromothiophene-2-carbaldehyde, (c) 5-(5-bromothiophen-2-yl)thiophene-2-carbaldehyde, (d) malononitrile, TEA, CHCl₃

3.2. Electrochemistry.

The redox behavior and energies of the frontier molecular orbitals were studied by cyclic voltammetry. The information that is directly obtained from cyclic voltammetry is the oxidation and reduction potential. For convenience we have converted these potentials into approximate HOMO and LUMO energies using the known oxidation potential and HOMO energy for ferrocene (HOMO = -5.1 eV). This gives a correlation between the energy required to add (remove) one electron to (from) a molecule, the standard reduction (oxidation) potential and the energy of the LUMO (HOMO) have been used to estimate the energy levels of the frontier orbitals.⁴⁸ The measurements were performed in CH₂Cl₂ containing 0.1 M n-Bu₄NPF₆ as a supporting electrolyte. As noted above, the molecular orbital energies are calculated from electrochemical results calibrated with ferrocene with

a value of 5.1eV (Table 1) and summarized for the two series of compounds in Figures 2 and 3, respectively.

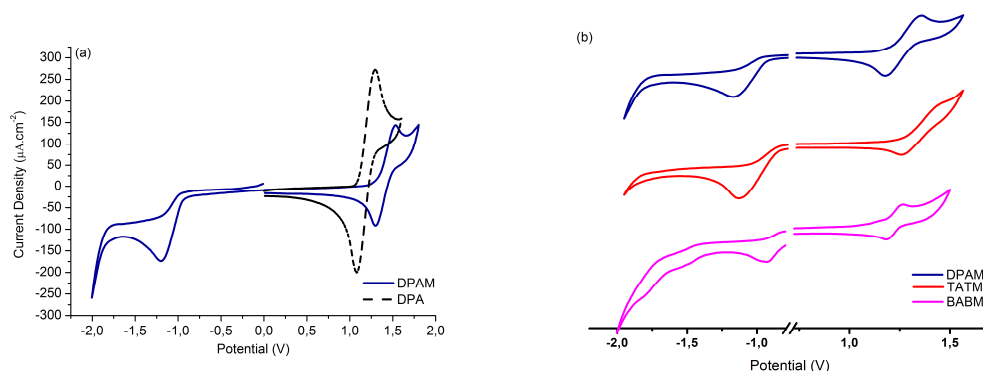


Figure 1. Cyclic voltammograms of (a) DPA-DPAM and (b) DPAM, TATM, BABM in 0.1 M Bu₄NPF₆/ CH₂Cl₂ at a scan rate of 50 mV/s.

In Figure 1a the cyclic voltammograms of DPA and DPAM are shown. The dicyanovinyl end-capped chromophore (DPAM) has a higher oxidation potential than that of the unsubstituted analogue (DPA), which translates to a lower HOMO level for the dicyanovinyl substituted compound. The same trend was observed for all the model compounds studied in this work. A lower-lying HOMO of the DCV substituted compounds is consistent with presence of the electron withdrawing dicyanovinyl units as compared to the control compounds. All of the control compounds without DCV show well-defined oxidation features; however, no cathodic reduction processes were recorded, which is different from the dicyanovinyl-end capped chromophore (see Supporting Information, Figure S1). The LUMO energies of the control compounds were obtained by subtracting the optical bandgaps from the electrochemical oxidation data. The LUMO energy levels show similar values in the range of -3.30 ± 0.10 eV. In Figure 2 the HOMO and LUMO energy levels are summarized for the directly-linked series of compounds. The scheme shows that the variation in the HOMO level is very small throughout this series (~ 0.4 eV) while for the LUMO level variations exceeding 1eV are observed. This is consistent with the electron-withdrawing nature of the DCV groups, which mostly affect the LUMO. In addition, the nature of the π -conjugated spacer between DCV and the central anthracene unit also affects the LUMO level, while leaving the HOMO energy

largely unchanged. The trends in the HOMO and LUMO levels can be understood when considering the results of electronic structure calculations. DFT calculations were performed using the M062X functional combined with a cc-pVDZ basis set in the Gaussian'09 program package.⁵⁴ The effect of the introduction of DCV units in the directly linked chromophores is clearly illustrated when comparing the shape and localization of the HOMO and LUMO for DPA and DPAM in Figure 4.

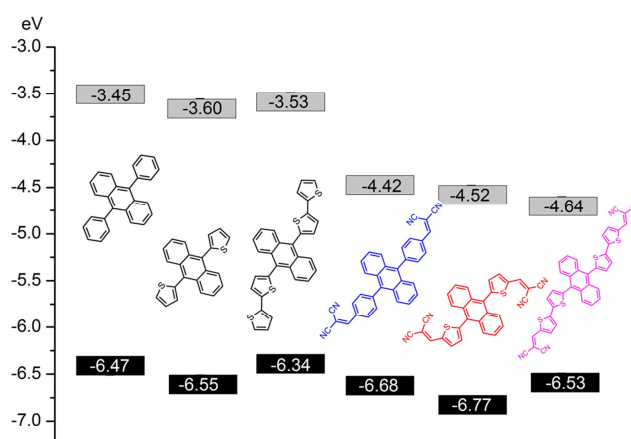


Figure 2. Energy levels of the control compounds and chromophores in directly-linked chromophores obtained by CV.

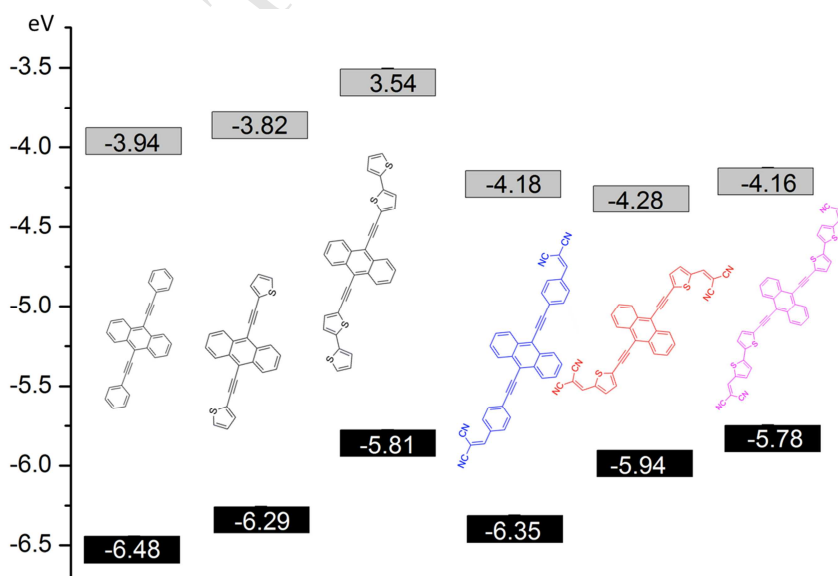


Figure 3: Energy levels of the control compounds and chromophores in ethynyl-linked chromophores obtained by CV.

For DPA, both the HOMO and LUMO are mostly localized on the anthracene unit and the electronic properties are almost not affected by the rest of the molecule. While the HOMO in DPA is largely unchanged when going to DPAM, the LUMO is now almost completely localized on the DCV units and the π -spacer. More detailed inspection shows that while the original anthracene LUMO is still present in DPAM (and has the same energy as in DPA), the DCV units contribute to a higher lying orbital on the outer parts of the molecule and pull the energy of this orbital below the anthracene LUMO. As is clearly seen in Figure 4, the LUMO spreads over both the DCVs and the π -spacer, but has very little density on the anthracene, again due to the large dihedral angle. An interesting trend can be observed when comparing the HOMO energy of DPAM and TATM. Thiophene is considered a better donor than benzene, however, the HOMO level of TATM is lower (more negative) than that of DPAM. This is caused by subtle differences in the dihedral angles between the central anthracene and the phenyl or thiophene. As can be seen in Table, for the thiophene containing side chains the dihedral angle is very close to 90 degrees and there is almost no mixing between the HOMO on anthracene and those on the thiophenes. For the DPAM, the angle is smaller and hence the large (but still small) mixing between the states on anthracene and the phenyl-containing side chain lead to slightly less negative HOMO levels.

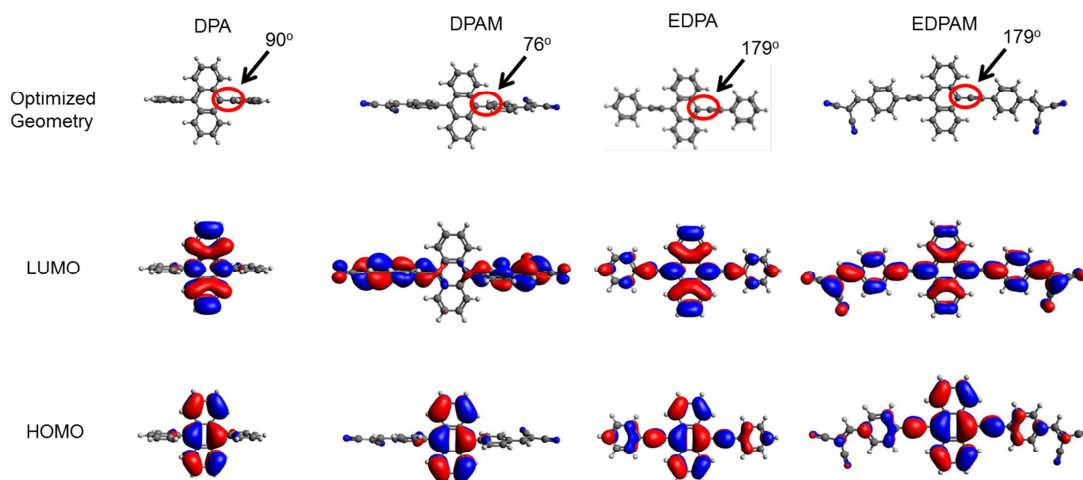


Figure 4. Optimized geometries, Frontier molecular orbitals HOMO and LUMO of DPA, DPAM, EDPA and EDPAM. Calculations were carried out at DFT (M062X/cc-pVDZ) level; dihedral angles between the planes of donor unit and linker unit are indicated by red circle.

The breaking of the π -conjugation by the strong deviations from planarity for the directly linked molecules can be overcome by the introduction of an ethynyl unit in the π -spacer. This reduces the steric interaction that leads to this conjugation breaking (Figure 4). Consequently, the ethynyl linked series of compounds have an almost fully planar conformation. This is reflected in the oxidation and reduction potentials that are summarized in Figure 3. Now, both the HOMO and LUMO energies change when structural changes are made in the outer parts of the molecules, even for the control compounds without DCV units. This indicates that the DCV units should contribute to both the HOMO and the LUMO. This is confirmed by the DFT calculations as seen in Figure 4. For EDPA both the HOMO and LUMO are fully delocalized over the whole molecule. The introduction of DCV in EDPAM changes this to some extent. The HOMO becomes more localized towards the anthracene while the LUMO is pulled to the outer parts of the molecule. This is directly reflected in the oxidation potential, which increases on introduction of DCV (see Figure 4). The LUMO level is considerably lowered by the introduction of the DCV units, as expected. In the other ethynyl-linked

compounds the nature of the π -spacer also affects both the HOMO and LUMO because it contributes to both of these orbitals that are now delocalized along the whole backbone of the molecule (See Table S1).

Table 1. Optical and electrochemical properties of chromophores.

| Chromophore | Abs _{max} (nm) ^a | ϵ_{max} (M ⁻¹ cm ⁻¹) | PL _{max} (nm) ^b | Eg ^{op} (eV) ^c | E _{HOMO} (eV) | E _{LUMO} (eV) | Eg ^{EC} (eV) ^d |
|-------------|--------------------------------------|---|-------------------------------------|------------------------------------|------------------------|------------------------|------------------------------------|
| DPAM | 390 | 16 x 10 ³ | 605 | 2.54 | -6.68 | -4.42 | 2.26 |
| TATM | 381 | 60 x 10 ³ | 587 | 2.51 | -6.77 | -4.52 | 2.25 |
| BABM | 453 | 23 x 10 ³ | 633 | 2.44 | -6.53 | -4.64 | 1.89 |
| EDPAM | 537 | 20 x 10 ⁴ | 587 | 2.17 | -6.35 | -4.18 | 2.17 |
| ETATM | 515 | 36 x 10 ⁴ | 620 | 2.02 | -5.94 | -4.28 | 1.66 |
| EBABM | 521 | 47 x 10 ⁴ | 634 | 1.98 | -5.78 | -4.16 | 1.62 |

^a First real maximum in spectrum, this does not directly correspond to the lowest electronic state. ^b From photoluminescence spectra in supporting information. ^c Energy gap determined from the onset of the optical absorption. ^d Energy gap from CV data.

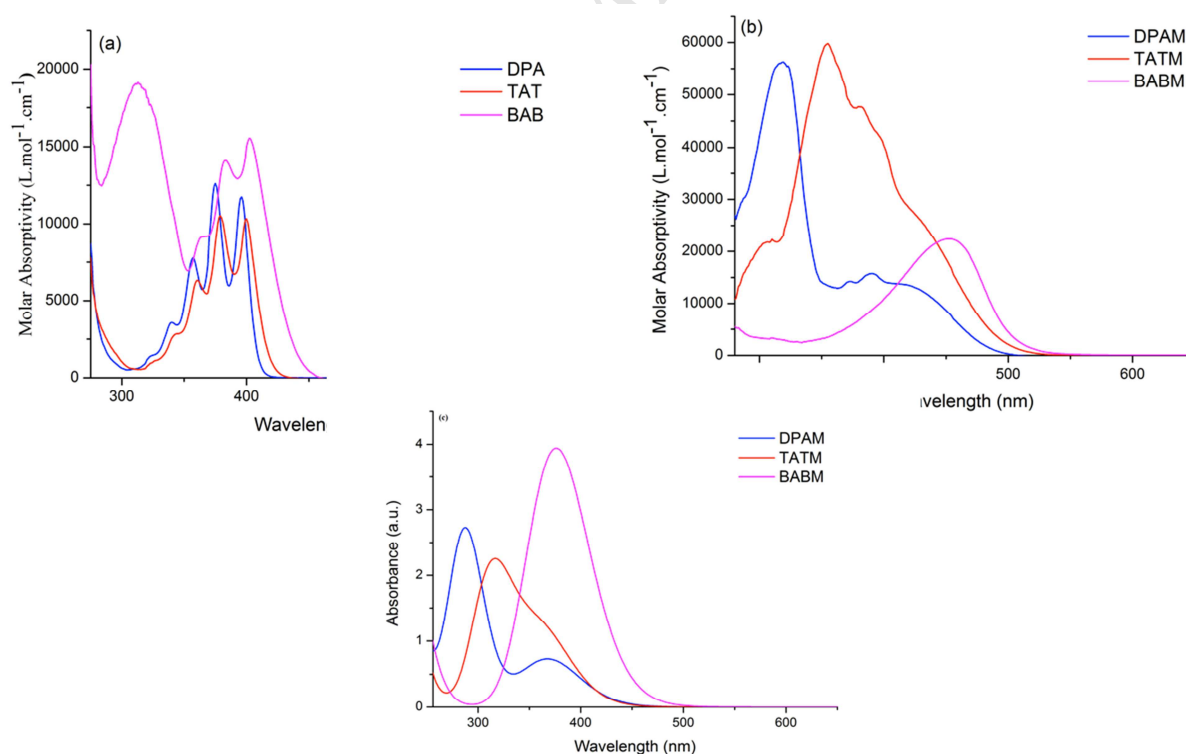


Figure 5. The optical absorption spectra of (a) control compounds and (b) DLCs chromophores (DPAM, TATM, BABM) in CH_2Cl_2 solution (c) Theoretical simulation of the UV-vis absorption spectra for DLCs chromophores (DPAM, TATM, BABM).

3.3. Optical Properties.

In Figure 5, the absorption spectra of the directly linked chromophore series are shown, together with those of the control compounds without DCV. The spectral data obtained from these spectra and the fluorescence emission spectra in the supporting information are summarized in Table 1.

In the unsubstituted analogues multiple absorption maxima are observed in the absorption spectra which are associated with the π - π^* transition of anthracene core. The characteristic vibrational fine structure of the isolated anthracene group confirms the results from the calculations described above that the introduction of bulky substituents to the 9 and 10 positions on the anthracene results in a nonplanar conformation with restricted π -electron delocalization. Therefore, the absorption spectrum is largely determined by the anthracene unit. Introduction of the electron withdrawing DCV groups leads to considerable red shifts in the absorption spectra for all chromophores. At the same time, the absorption spectra lose the characteristic vibrational fine structure that was observed in the unsubstituted analogues. This shows that the nature of the excited state changes, from a localized excitation on the anthracene to a delocalized excitation to which the anthracene, π -spacer and the DCV all contribute. The optical band gaps, taken as the onset of the absorption, are found to be 2.48 eV for DPAM with the benzene linker, 2.45 eV for TATM with the thiophene linker, 2.42 eV for BABM with the dithiophene linker. The emergence of a shoulder in the absorption spectra of DPAM and less pronounced in TATM could be an indication of an intramolecular charge transfer between the electron rich anthracene core and the electron poor dicyanovinyl end groups. In order to obtain more information on the nature of the different features in the UV/Vis spectra of the chromophores studied in this work

we have performed time-dependent DFT calculations.⁵⁶⁻⁵⁷ A variety of density functionals and basis sets (GGA (BP86), Hybrid (B3LYP) and meta-GGA (M06-2X)) were compared in this study to establish the best functional for the calculation of the optical properties of the DCV substituted compounds as described in the supporting information. In agreement with extensive benchmarks of DFT functionals for the calculation of excitation energies it is found that M06-2X performs very well.⁵⁸⁻⁵⁹

Table 2. Calculated and experimental transition energies (ΔE in eV), calculated oscillator strengths (f) and composition of excited state.

| Compound | ΔE (exp.) in eV | ΔE (calc.) in eV | f (calc.) | Composition of excited state |
|----------|-------------------------------|--------------------------------|----------------|--|
| DPAM | 2.92 | 3.33 | 0.38 | $0.61(\text{H}\rightarrow\text{L}) + 0.33(\text{H}\rightarrow\text{L}+2)$ |
| | 3.23 | 3.60 | 0.12 | $-0.32(\text{H}\rightarrow\text{L}) + 0.61(\text{H}\rightarrow\text{L}+2)$ |
| | 3.99 | 4.31 | 1.60 | $0.49(\text{H}-3\rightarrow\text{L}) - 0.48(\text{H}-2\rightarrow\text{L}+1)$ |
| TATM | 2.77 | 3.42 | 0.67 | $0.14(\text{H}-2\rightarrow\text{L}) - 0.14(\text{H}-1\rightarrow\text{L}+1) + 0.68(\text{H}\rightarrow\text{L}+2)$ |
| | 3.17 | 3.95 | 1.31 | $-0.48(\text{H}-2\rightarrow\text{L}) + 0.48(\text{H}-1\rightarrow\text{L}+1) + 0.19(\text{H}\rightarrow\text{L}+2)$ |
| | 3.56 | 5.31 | 1.31 | $-0.21(\text{H}-5\rightarrow\text{L}+2) + 0.45(\text{H}-3\rightarrow\text{L}+2) + 0.50(\text{H}\rightarrow\text{L}+3)$ |
| BABM | 2.72 | 3.26 | 1.91 | $0.41(\text{H}-2\rightarrow\text{L}) + 0.40(\text{H}-1\rightarrow\text{L}+1) - 0.39(\text{H}\rightarrow\text{L}+2)$ |
| | 3.00 | 3.43 | 0.59 | $0.49(\text{H}-2\rightarrow\text{L}+1) + 0.49(\text{H}-1\rightarrow\text{L})$ |
| | | 3.54 | 0.10 | $0.28(\text{H}-2\rightarrow\text{L}) + 0.28(\text{H}\rightarrow\text{L}) + 0.58(\text{H}\rightarrow\text{L})$ |
| EDPAM | 2.30 | 2.54 | 1.75 | $-0.11(\text{H}-1\rightarrow\text{L}+1) + 0.68(\text{H}\rightarrow\text{L}) + 0.15(\text{H}\rightarrow\text{L}+2)$ |
| | 3.25 | 3.65 | 0.32 | $-0.16(\text{H}-2\rightarrow\text{L}) + 0.12(\text{H}-1\rightarrow\text{L}+1) + 0.65(\text{H}\rightarrow\text{L}+2)$ |
| | | 4.00 | 0.82 | $0.61(\text{H}-2\rightarrow\text{L}) - 0.22(\text{H}-1\rightarrow\text{L}+1) + 0.18(\text{H}\rightarrow\text{L}+2)$ |
| ETATM | 2.54 | 2.43 | 1.94 | $0.68(\text{H}\rightarrow\text{L}) - 0.13(\text{H}-1\rightarrow\text{L}+1) + 0.11(\text{H}\rightarrow\text{L}+2)$ |
| | 3.75 | 3.53 | 0.36 | $0.62(\text{H}\rightarrow\text{L}+2) + 0.24(\text{H}-2\rightarrow\text{L}) + 0.18(\text{H}-1\rightarrow\text{L}+1)$ |
| | 4.72 | 3.80 | 0.50 | $0.59(\text{H}-2\rightarrow\text{L}) - 0.27(\text{H}\rightarrow\text{L}+2) + 0.19(\text{H}-1\rightarrow\text{L}+1)$ |
| EBABM | 2.40 | 2.39 | 2.69 | $-0.18(\text{H}-1\rightarrow\text{L}+1) + 0.64(\text{H}\rightarrow\text{L}) - 0.18(\text{H}\rightarrow\text{L}+2)$ |
| | 2.92 | 3.24 | 0.39 | $0.27(\text{H}-2\rightarrow\text{L}) - 0.28(\text{H}-1\rightarrow\text{L}+1) + 0.56(\text{H}\rightarrow\text{L}+2)$ |
| | | 3.59 | 0.45 | $0.48(\text{H}-2\rightarrow\text{L}) - 0.28(\text{H}-1\rightarrow\text{L}+1) - 0.33(\text{H}\rightarrow\text{L}+2)$ |

In Table 2, the calculated transition energies of the lowest three excited states with an oscillator strength (f) larger than 0.1 are listed, together with the composition of the excited states. The experimental values for the low-lying transition were

obtained from fitting the absorption spectra with multiple Gaussian peaks since they typically consist of multiple close lying transitions (see Supporting Information Figure S7). For DPAM the lowest excited state consists mostly of excitation of an electron from HOMO to LUMO. From the discussion above on the localization of the HOMO and LUMO on the anthracene and dicyanovinyl parts of the molecule it is clear that the lowest allowed transition for DPAM (corresponding to the shoulder in the absorption spectrum at 425 nm) has a substantial charge transfer character. For the other two directly linked chromophores, TATM and BABM the observation is rather different. In this case the lowest excited state does not contain any HOMO-LUMO character but excitations from other orbitals are dominant. From a detailed inspection of the different excited states it was found that in both TATM and BABM a charge transfer excited state similar to that in DPAM exists but with negligible oscillator strength so it does not contribute to the observed absorption spectrum. The large contribution of HOMO-LUMO transition in the lowest excited state for DPAM leads to considerable CT character in this case. The other transitions involved in the allowed excited states for the directly-linked compounds involve orbitals that are localized on the same unit, as can be inferred from Table 2 and the orbital pictures that are shown in Figure S5 in the supporting information. As an example, for TATM in the (H->L+2) contribution both orbitals are localized on the anthracene units, while for the other two contributions (H-2->L and H-1->L+1) both orbitals are localized on the DCV and the pi-spacer. The same trend is also observed for all other transitions in these three compounds. From the data for the lowest three calculated transitions in Table 2 it also becomes clear that the appearance of the experimental absorption spectra for the directly linked chromophores results from several close lying transitions. This is also true for instance for BABM where contributions from different electronic states to the experimental spectrum are less obvious than in DPAM and TATM. In order to directly compare the experimental spectra we have used the 30 lowest calculated transitions from the TDDFT calculations to construct simulated absorption spectra, using a Gaussian broadening of the absorption bands of 0.25 eV. The result of this

simulation is shown in Figure 5c. Overall, the agreement of the general shape of the spectra is rather good, with a consistent blue shift of the spectra compared to the experimental data. The latter is attributed to the absence of any environment effect in the calculations, while the experiments were done in CH_2Cl_2 solution. In the second series of chromophores, ethynyl groups containing carbon-carbon triple bonds were introduced in the π -spacer to enhance the effective conjugation over the molecule by removing the steric interaction between the anthracene core and the aromatic bridges. As discussed above, the viability of this approach is confirmed by geometry optimizations that show that the ethynyl-inserted systems are planar (see Figure 4). The absorption spectra of the control compounds without DCV, shown in Figure 6a, clearly show the effect of the insertion of the ethynyl units.

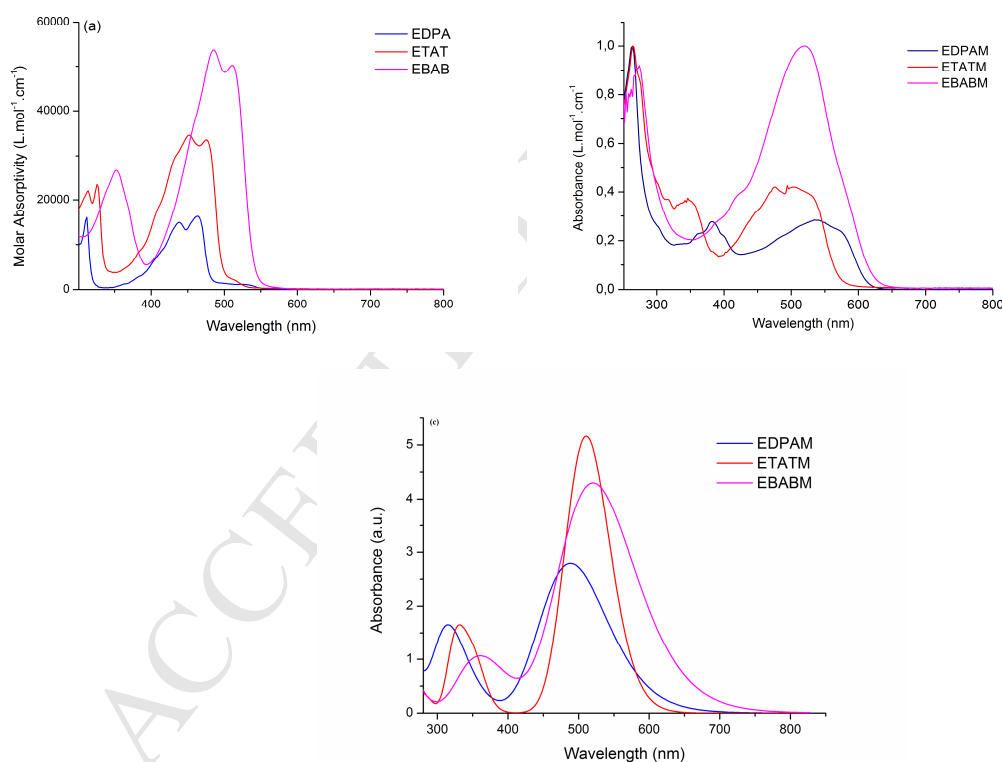


Figure 6. The optical absorption spectra of (a) control compounds and (b) ELCs chromophores (EDPAM, ETATM, EBABM) in CH_2Cl_2 solution (c) Theoretical simulation of the UV-vis absorption spectra for ELCs chromophores (EDPAM, ETATM, EBABM).

The absorption bands shift to lower energy, become broadened and lose the vibrational structure as compared to the directly linked control compounds (Figure 5a). Inclusion of the DCV units leads to a pronounced red-shift in the absorption spectrum in all three compounds, similar as observed for the directly linked chromophores. The optical band gaps calculated from the onset of the π - π^* transition were found to be 2.17, 2.02 and 1.98 eV for EDPAM, ETATM and EBABM, respectively. This trend reflects the more electron-rich nature of the thiophene group, as compared to the phenyl group, leading to a higher lying HOMO and hence a decreased energy gap. Addition of a second thiophene ring in EBABM further increases the HOMO (see Figure 3) but apparently also moves the LUMO level to higher energy, resulting in only a minor decrease in the energy gap. DFT calculations for the ethynyl linked series show that the lowest allowed transition is in all cases dominated by HOMO-LUMO excitation. As was discussed above, both the HOMO and the LUMO for the ethynyl linked chromophores are rather delocalized, but the HOMO still has more density on the anthracene while the LUMO is localized more towards the dicyanovinyl. Therefore, the lowest transitions in EDPAM, ETATM and EBABM exhibit small charge transfer character (see below). In the case of the ethynyl-linked chromophores the DFT calculations show that the different electronic transitions are well-separated, with roughly 1 eV difference between the lowest two excited states in all cases. The shape simulated absorption spectra are also in good agreement with the experimental spectra (Figure 6c), although again the relative intensities for the different compounds are not reproduced.

3.4. Charge transfer character in the excited state

The charge transfer character in the excited states can be more clearly identified by comparing the electron density in the ground state and the excited states.⁴⁴ In Figure 7 the change in the charge distribution upon excitation to the lowest (allowed) excited state is shown for all six chromophores. These changes in charge distribution were obtained by taking the difference in the sum of the Mulliken charges for a specific fragment (anthracene, ethynyl, phenyl, thiophene and dicyanovinyl) of the molecule in the ground and excited state. The figure clearly illustrates the significant charge transfer character for

the lowest excited state in DPAM; a significant amount of negative charge moves from the anthracene unit towards the dicyanovinyl units in the outer parts of the molecule. For TATM and BABM there is hardly any shift in charge upon excitation, which clearly shows that there is very little charge transfer character in the lowest allowed excited state. This is consistent with the absence of HOMO-LUMO character in this excited state. For all ethynyl-linked chromophores (EDPAM, ETATM and EBABM) the picture is similar. There is a clear shift of electrons from the anthracene towards the dicyanovinyl units but the amount of charge is considerably less than for DPAM (0.1-0.2 e vs. ~0.4 e for DPAM). This can be understood when the shape of the HOMO and LUMO orbitals are considered. Both the HOMO and the LUMO are delocalized, but with some extra density on the anthracene for the HOMO and some extra density on the dicyanovinyl for the LUMO. Since the lowest excited state is dominated by a transition from the HOMO to the LUMO in all of these chromophores, excitation leads to a small shift in charge upon excitation.

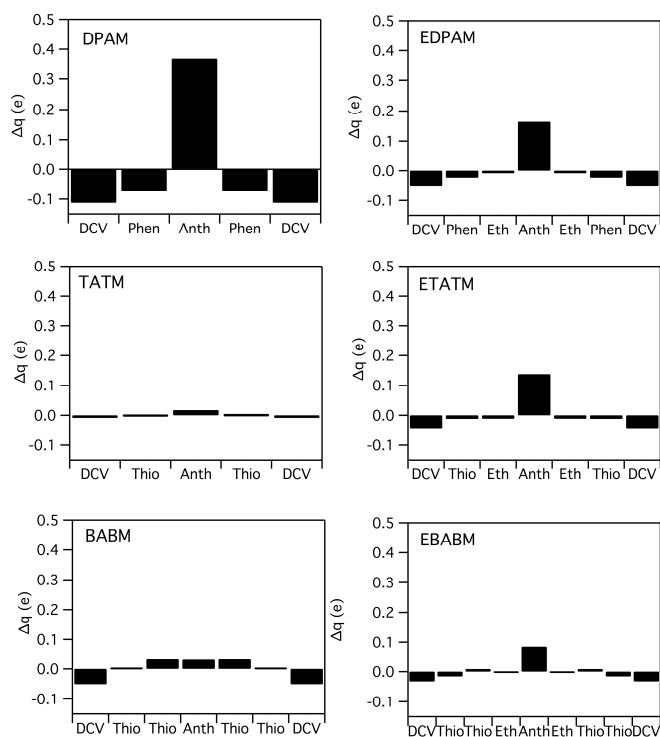


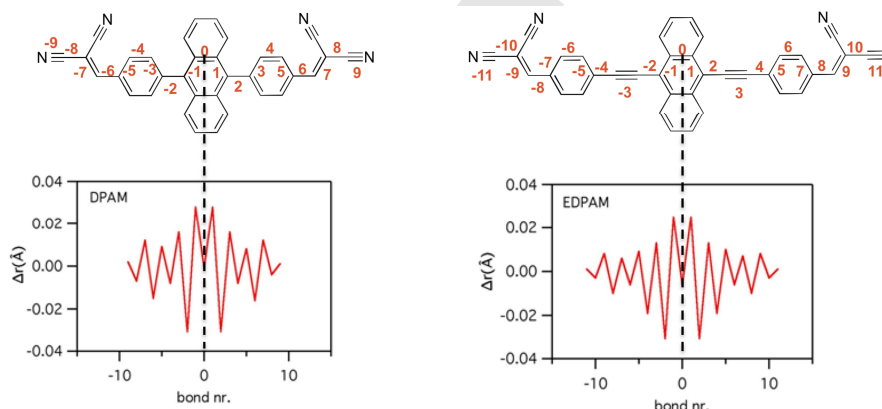
Figure 7. Change in the charge density on the different sub-units in the chromophores upon excitation to the first excited state as obtained from a Mulliken population analysis.

3.5. Stokes shift and geometric structure reorganization.

Excitation of a chromophore to an excited state generally leads to changes in the geometry of the molecule. Such geometry changes are reflected in the Stokes shift; the difference between the absorption and emission maxima. These shifts can be obtained from experimental data but can also be calculated by optimization of the geometry of the excited state using time-dependent density functional theory. The experimental and calculated absorption and emission energies are listed in Table 3 together with the Stokes shift obtained from these data. Both in the experimental and the calculated data there is a clear distinction in the Stokes shift for the DLCs and ELCs series. Although the difference is more pronounced in the calculations than in the experimental data, it is clear that the Stokes shift is larger for the directly linked series than it is for the ethynyl linked series. This points to larger geometric structure reorganization upon excitation for the directly linked series than for the ethynyl linked chromophores. In the directly linked chromophores the geometric structure reorganization can roughly be divided in two parts; planarization and a transition from aromatic and quinoidal bonding patterns. From the geometry optimization it becomes clear that relaxation of the geometry in the directly linked chromophores leads to a significant decrease in the dihedral angle between the anthracene and the neighboring phenyl or thiophene groups (see Table 3). This partial planarization results in an increased degree of conjugation in the excited state, and hence a significant Stokes shift. Apart from the planarization there are many other degrees of freedom by which geometry relaxation can take place after excitation. Most importantly for conjugated molecules, deformations in the carbon-carbon bond lengths occur upon excitation. In the ground state a sequence of (formally) single and multiple bonds can be followed through the molecule where there are distinct differences in the bond length; i.e. a bond-length alternation can be observed. This bond-length alternation generally becomes less upon transition to the excited state due to the quinoidal bonding patterns. This geometry deformation leads to a Stokes shift. The calculated Stokes shift due to all geometry deformations is roughly 1 eV for the directly linked chromophores.

Table 3. Calculated and experimental absorption and emission energies (ΔE in eV).

| Compound | ΔE_{abs} (exp. in eV) | ΔE_{em} (exp. in eV) | Stokes shift (exp.) | ΔE_{abs} (calc. in eV) | ΔE_{em} (calc. in eV) | Stokes shift (calc.) | ϕ_{gs} (deg.) | ϕ_{es} (deg.) |
|----------|---|--|---------------------------|---|--|----------------------------|------------------------------|------------------------------|
| DPAM | 2.92 | 2.15 | 0.77 | 3.33 | 2.51 | 0.82 | 80 | 51 |
| TATM | 2.77 | 2.16 | 0.61 | 3.42 | 2.34 | 1.08 | 90 | 45 |
| BABM | 2.72 | 2.04 | 0.68 | 3.26 | 2.32 | 0.94 | 90 | 48 |
| EDPAM | 2.30 | 2.13 | 0.17 | 2.54 | 2.19 | 0.35 | 0 | 0 |
| ETATM | 2.54 | 1.98 | 0.56 | 2.43 | 2.08 | 0.35 | 0 | 0 |
| EBABM | 2.40 | 1.89 | 0.51 | 2.39 | 2.01 | 0.38 | 0 | 0 |

**Figure 8.** Change in the C-C bond lengths along the chromophore backbone upon excitation to the lowest excited state. The numbering of the bonds is indicated in the scheme.

For the ethynyl-linked chromophores the Stokes shift is overall significantly smaller, both in the experiments and in the calculations. The main difference between the directly linked series and the ethynyl linked series is that the ethynyl linked chromophores are fully planar in the ground state. Therefore no planarization can occur in the excited state. Therefore, we conclude that in the directly linked series, the larger Stokes shift is due to

planarization of the non-planar molecule. In the ethynyl-linked series both the ground state and the excited state are fully planar and the only geometry deformation that can occur is in the bond length. As can be seen in Figure 8 and Figure S4, the changes in the C-C bond lengths are similar to those in the directly-linked chromophores. In all cases the largest change in bond length (0.035 Å) is found in the bond connecting the central anthracene unit with the rest of the molecule. Generally, the deformations become less pronounced in the outer parts of the chromophores, which is consistent with the changes in charge distribution on excitation.

4. Summary and Conclusions

In this work, we have presented a combined experimental and theoretical characterization of the structural and electronic properties of Acceptor-Donor-Acceptor (A-D-A) type chromophores, incorporating dicyanovinyl (DCV) units as the terminal acceptor moieties. DCV units are connected to the donor unit through different π -spacers. Specific emphasis is placed on the structure of the benzene- and thiophene-based π -spacer and the effect of adding an additional “ethynyl” unit that leads to more planar geometries. A comparison between the experimental and theoretical work leads to detailed insight in the relationship between the molecular structure and electronic structure of A-D-A type chromophores. It is shown that for compounds that exhibit large deviations from planarity, the orbitals are rather localized on different subunits. However, the charge transfer character in most allowed transitions remains small because generally, only transitions between orbitals on the same units are involved. The more planar structures obtained after inserting ethynyl units exhibit more delocalized orbitals, leading to a significant red-shift in the absorption spectra.

While A-D-A molecular design approach allowed us to systematically lower the LUMO energy levels of the target chromophores, HOMO-LUMO gap is not directly related to the absorption properties. This is due to the subtle effect that the molecular geometry has on the shape and delocalization of the orbitals, especially for non-planar compounds. In the case of planar π -conjugated compounds the HOMO-LUMO transition is dominating the optical absorption but due to the more delocalized nature of the frontier orbitals the energy levels of the HOMO and LUMO cannot be controlled individually.

In order to establish the suitability of the new materials presented here for photovoltaic devices we have performed preliminary photoconductivity experiments on drop-casted blends with C60-PCBM. While clear evidence of photoinduced charge separation was observed, the experiments are complicated by the high tendency of these materials to form crystalline domains. This could be resolved by using physical vapor deposition and we are currently working in this direction.

Acknowledgements

This work is supported by the Netherlands Organization for Scientific Research (NWO) through an VIDI grant to FCG and by the European Research Council FP7 ERC grant agreement no. 240299.

References and Notes

1. Nielsen, C.; Turbiez, M.; McCulloch I. *Adv. Mater.* **2013**, 25, 1859-1880.
2. Zhang J.; Deng D.; He C.; He Y.; Zhang M.; Zhang Z. G.; Zhang Z.; Li Y. *Chem. Mater.* **2011**, 23, 817-822.
3. Kulkarni A. P.; Tonzola C. J.; Babel A.; Jenekhe S. A. *Chem. Mater.* **2004**, 16, 4556-4573.
4. Takacs C. J.; Sun Y.; Welch G. C.; Perez L. A.; Liu X.; Wen, W.; Bazan G. C.; Heeger A. *J. Am. Chem. Soc.* **2012**, 134, 16597-16606.
5. Estrada L. A.; Liu D. Y.; Salazar D. H.; Dyer A. L.; Reynolds J. R. *Macromolecules* **2012**, 45, 8211-8220.
6. Beaujuge P. M.; Frechet J. M. J. *J. Am. Chem. Soc.* **2011**, 133, 20009-20029.
7. Lin Y.; Li Y.; Zhan X. *Chem. Soc. Rev.* **2012**, 41, 4245-4272.
8. Wen L.; Heth C. L.; Rasmussen S. C. *Phys. Chem. Chem. Phys.* **2014**, 16, 7231-7240.
9. Tlach B. C.; Tomlinson A. L.; Bhuwarka A.; Jeffries-El M. *J. Org. Chem.* **2011**, 76, 8670-8681.
10. Mishra A.; Bäuerle P. *Angew. Chem. Int. Ed.* **2012**, 51, 2020-2067.
11. Yao H.; Ye L.; Zhang H.; Li S.; Zhang S.; Hou J. *Chem. Rev.* **2016**, 116, 7397-7457.
12. Guide M.; Pla S.; Sharenko A.; Zalar P.; Fernández-Lázaro F.; Sastre-Santos Á. ; Nguyen T. Q. *Phys. Chem. Chem. Phys.* **2013**, 15, 18894-18899.

13. Chen Y. H.; Lin L. Y.; Lu C. W.; Lin F.; Huang Z. Y.; Lin H. W.; Wang P. H.; Liu Y. H.; Wong K. T.; Wen J.; Miller D. J.; Darling S. B. *J. Am. Chem. Soc.* **2012**, 134, 13616-13623.
14. Wrackmeyer M. S.; Hummert M.; Hartmann H.; Riede M. K.; Leo K. *Tetrahedron* **2010**, 66, 8729-8733.
15. Zhang S.; Wang X.; Tang A.; Huang J.; Zhan C.; Yao J. *Phys. Chem. Chem. Phys.* **2014**, 16, 4664-4671.
16. Liu Y.; Wan X.; Wang F.; Zhou J.; Long G.; Tian J.; You J.; Yang Y.; Chen Y. *Adv. Energy Mater.* **2011**, 1, 771-775.
17. Bürckstümmer H.; Kronenberg N. M.; Gsänger M.; Stolte M.; Meerholz K.; Würthner F. *J. Mater. Chem.* **2010**, 20, 240-243.
18. Roquet S.; Cravino A.; Leriche P.; Alévêque O.; Frère P.; Roncali J. *J. Am. Chem. Soc.* **2006**, 128, 3459-3466.
19. Bagnis D.; Beverina L.; Huang H.; Silvestri F.; Yao Y.; Yan H.; Pagani G. A.; Marks T. J.; Facchetti A. *J. Am. Chem. Soc.* **2010**, 132, 4074-4075.
20. Luponosov Y. N.; Min J.; Solodukhin A. N.; Kozlov O. V.; Obrezkova M. A.; Peregudova S. M.; Ameri T.; Chvalun S. N.; Pshenichnikov M. S.; Brabec C. J.; Ponomarenko S. A. *Organic Electronics* **2016**, 32, 157-168.
21. Du J.; Fortney A.; Washington K. E.; Bulumulla C.; Huang P.; Dissanayake D.; Biewer M.C.; Kowalewski T.; Stefan M. C. *ACS Appl. Mater. Interfaces* **2016**, 8, 33025-33033.
22. Osaka I.; Shimawaki M.; Mori H.; Doi I.; Miyazaki E.; Koganezawa T.; Takimiya K. *J. Am. Chem. Soc.* **2012**, 134, 3498-3507.
23. Ying W.; Guo F.; Li J.; Zhang Q.; Wu W.; Tian H.; Hua J. *ACS Appl. Mater. Interfaces* **2012**, 4, 4215-4224.
24. Pappenfus T. M.; Schneiderman D. K.; Casado J.; Navarrete J. T. L.; Ruiz Delgado M. C.; Zotti G.; Vercelli B.; Lovander M. D.; Hinkle L. M.; Bohnsack J. N.; Mann K. R. *Chem. Mater.* **2011**, 23, 823-831.
25. Lelièvre A.; Blanchard P.; Rousseau T.; Roncali J. *Org. Lett.* **2011**, 13, 3098-3101.
26. Gupta A.; Ali A.; Bilic A.; Gao M.; Hegedus K.; Singh B.; Watkins S. E.; Wilson G. J.; Bach U.; Evans R. A. *Chem. Commun.* **2012**, 48, 1889-1891.

27. Chiu S. W.; Lin L. Y.; Lin H. W.; Chen Y. H.; Huang Z. Y.; Lin Y. T.; Lin F.; Liu Y. H.; Wong K. T. *Chem. Commun.* **2012**, 48, 1857-1859.
28. Sonar P.; Singh S. P.; Leclère P.; Surin M.; Lazzaroni R.; Lin T. T.; Dodabalapur A.; Sellinger A. *J. Mater. Chem.* **2009**, 19, 3228-3237.
29. He G.; Li Z.; Wan X.; Liu Y.; Zhou J.; Long G.; Zhang M.; Chen Y. *J. Mater. Chem.* **2012**, 22, 9173-9180.
30. Salzner U. *J. Phys. Chem. B* **2002**, 106, 9214-9220.
31. Salzner U.; Kose M. E. *J. Phys. Chem. B* **2002**, 106, 9221-9226.
32. Singh M.; Kurchania R.; Mikroyannidis J. A.; Sharma S. S.; Sharma G. D. *J. Mater. Chem. A*, **2013**, 1, 2297-2306.
33. Li C.; Chen Y.; Zhao Y.; Wang H.; Zhang W.; Li Y.; Yang X.; Ma C.; Chen L.; Zhu X.; Tu Y. *Nanoscale* **2013**, 5, 9536-9540.
34. Lai Y.Y.; Yeh J. M.; Tsai C. E.; Cheng Y. J. *Eur. J. Org. Chem.* **2013**, 5076-5084.
35. Calbo J.; Arago J.; Oton F.; Lloveras V.; Mas-Torrent M.; Vidal-Gancedo J.; Veciana J.; Rovira C.; Orti E. *Chem. Eur. J.* **2013**, 19, 16656-16664.
36. Steinberger S.; Mishra A.; Reinold E.; Levichkov J.; Uhrich C.; Pfeiffer M.; Bäuerle P. *Chem. Commun.* **2011**, 47, 1982-1984.
37. Qi T.; Liu Y.; Qiu W.; Zhang H.; Gao X.; Liu Y.; Lu K.; Du C.; Yu G.; Zhu D. *J. Mater. Chem.* **2008**, 18, 1131-1138.
38. Yang L.; Zhang S.; He C.; Zhang J.; Yao H.; Yang Y.; Zhang Y.; Zhao W.; Hou J. *J. Am. Chem. Soc.* **2017**, 139, 1958-1966.
39. Wu J.; Ma Y.; Wu N.; Lin Y.; Lin J.; Wang L.; Ma C. *Organic Electronics* **2015**, 23, 28-38.
40. Fitzner R.; Mena-Osteritz E.; Mishra A.; Schulz G.; Reinold E.; Weil M.; Körner C.; Ziehlke H.; Elschner C.; Leo K.; Riede M.; Pfeiffer M.; Uhrich C.; Bäuerle P. *J. Am. Chem. Soc.* **2012**, 134, 11064-11067.
41. Haid S.; Mishra A.; Uhrich C.; Pfeiffer M.; Bäuerle P. *Chem. Mater.* **2011**, 23, 4435-4444.

42. Fitzner R.; Reinold E.; Mishra A.; Mena-Osteritz E.; Ziehlke H.; Körner C.; Leo K.; Riede M.; Weil M.; Tsaryova O.; Weis A.; Uhrich C.; Pfeiffer M.; Bäuerle P. *Adv. Func. Mater.* **2011**, 27, 897-910.
43. Steinberger S.; Mishra A.; Reinold E.; Mena-Osteritz E.; Müller H.; Uhrich C.; Pfeiffer M.; Bäuerle P. *J. Mater. Chem.* **2012**, 22, 2701-2712.
44. Elschner C.; Schrader M.; Fitzner R.; Levin A. A.; Bäuerle P.; Andrienko D.; Leo K.; Riede M. *RSC. Adv.* **2013**, 3, 12117-12123.
45. Simon J.; Atherton J.C.C. *Synth. Commun.* **2001**, 31, 1799-1802.
46. Chen R.; Yang X.; Tian H.; Wang X.; Hagfeldt A.; Sun L. *Chem. Mater.* **2007**, 19, 4007-4015.
47. Colella S.; Mazzeo M.; Grisorio R.; Fabiano E.; Melcarne G.; Carallo S.; Angione M. D.; Torsi L.; Suranna G.P.; della Sala F.; Mastroilli P.; Gigli G. *Chem. Commun.* **2010**, 46, 6273-6275.
48. Khan M. S.; Al-Mandhary M. R. A.; Al-Suti M. K.; Al-Battashi F. R.; Al-Saadi S.; Ahrens B.; Bjernemose J.K.; Mahon M. F.; Raithby P.R.; Younus M.; Chawdhury N.; Köhler A.; Marseglia E. A.; Tedesco E.; Feederd N.; Teate S. *Dalton. Trans.* **2004**, 2377-2385.
49. Fraind A. M.; Tovar J. D. *J. Phys. Chem. B.* **2010**, 114, 3104-3116.
50. Swager T. M.; Gil C. J.; Wrighton M.S. *J. Phys. Chem.* **1995**, 99, 4886-4893.
51. Wang C.; Liu Y.; Ji Z.; Wang E.; Li R.; Jiang H.; Tang Q.; Li H.; Hu W. *Chem. Mater.* **2009**, 21, 2840-2845.
52. Cardona C. M.; Li W.; Kaifer A. E.; Stockdale D.; Bazan G.C. *Adv. Mater.* **2011**, 23, 2367-2371.
53. Beaujuge P. M.; Subbiah J.; Choudhury K. R.; Ellinger S.; McCarley T. D.; So F.; Reynolds J. R. *Chem. Mater.* **2010**, 22, 2093-2106.
54. Frisch M. J.; Trucks G. W.; Schlegel H. B.; Scuseria G. E.; Robb M.A.; Cheeseman J. R.; Scalmani G.; Barone V.; Mennucci B.; Petersson G. A.; Nakatsuji H.; Caricato M.; Li X.; Hratchian H.P.; Izmaylov A.F.; Bloino J.; Zheng G.; Sonnenberg J. L.; Hada M.; Ehara M.; Toyota K.; Fukuda R.; Hasegawa J.; Ishida M.; Nakajima T.; Honda Y.; Kitao O.; Nakai H.; Vreven T.; Jr. Montgomery J.A.; Peralta J. E.; Ogliaro F.; Bearpark M.; Heyd J.J.; Brothers E.;

- Kudin K. N.; Staroverov V.N.; Kobayashi R.; Normand J.; Raghavachari K.; Rendell A., Burant J. C; Iyengar S.S.; Tomasi J.; Cossi M.; Rega N.; Millam N.J.; Klene M.; Knox J. E.; Cross J. B.; Bakken V.; Adamo C.; Jaramillo J.; Gomperts R.; Stratmann R. E.; Yazyev O.; Austin A. J., Cammi R.; Pomelli C.; Ochterski J.W.; Martin R. L.; Morokuma K.; Zakrzewski V. G.; Voth G. A.; Salvador P.; Dannenberg J. J.; Dapprich S.; Daniels A. D.; Farkas Ö.; Foresman J. B.; Ortiz J.V.; Cioslowski J.; Fox D. J. *Gaussian, Inc.: Wallingford, CT, 2009.*
55. Fraind A. M.; Sini G.; Risko C.; Ryzhkov L. R.; Brédas J. L; Tovar J. D. *J. Phys. Chem. B* **2013**, 117, 6304-6317.
56. Estrada L. A.; Stalder R.; Abboud K. A.; Risko C.; Brédas J. L.; Reynolds J. R. *Macromolecules* **2013**, 46, 8832-8844.
57. Salman S.; Brédas J. L.; Marder S. R.; Coropceanu V.; Barlow S. *Organometallics* **2013**, 32, 6061-6068.
58. Leang S. S.; Zahariev F.; Gordon M. S. *J. Chem. Phys.* **2012**, 136, 104101-104101-11.
59. Zhao Y.; Truhlar D. G. *Theor. Chem. Account* **2008**, 120, 215–241.

Supplementary Materials

Electronic Supplementary Information (ESI) available: [Methods and materials, synthetic procedures and characterization details. DFT data for the optimize geometries, frontier orbitals, electronic structure.]